A single-layer approach for joint optimization of traffic signals and cooperative vehicle trajectories at isolated intersections

Liu, Meiqi; Zhao, Jing ; Hoogendoorn, Serge; Wang, Meng Wang

Important note
To cite this publication, please use the final published version (if applicable).
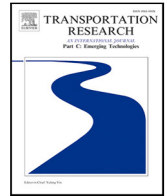Please check the document version above.

A single-layer approach for joint optimization of traffic signals and cooperative vehicle trajectories at isolated intersections☆

Meiqi Liu [a], Jing Zhao [a,b], Serge Hoogendoorn [a], Meng Wang [a,*]

[a] *Department of Transport & Planning, Delft University of Technology, Stevinweg 1, 2628 CN, Delft, The Netherlands*
[b] *Department of Traffic Engineering, University of Shanghai for Science and Technology, Shanghai, China*

A B S T R A C T

A joint control approach that simultaneously optimizes traffic signals and trajectories of cooperative (automated) vehicle platooning at urban intersections is presented in this paper. In the proposed approach, the signal phase lengths and the accelerations of the controlled platoons are optimized to maximize comfort and minimize travel delay within the signal cycle, subject to motion constraints on speeds, accelerations and safe following gaps. The red phases are initially considered as logic constraints, and then recast as several linear constraints to enable efficient solutions. The proposed approach is solved by mixed integer linear programming (MILP) techniques after linearization of the objective function. The generated outputs of the MILP problem are the optimal signal timings and the optimal accelerations of all vehicles. This joint control approach is flexible in incorporating multiple platoons and traffic movements under different traffic demand levels and it does not require prespecified terminal conditions on position and speed at the signal cycle tail. The performance of the proposed control approach is verified by simulation at a standard four-arm intersection under the balanced and unbalanced vehicle arrival rates from different arms, taking the released traffic movement numbers, turning proportions, signal cycle lengths and the controlled vehicle numbers into account. The simulation results demonstrate the platoon performance of the joint controller (such as split, merge, acceleration and deceleration maneuvers) under the optimal signals. Based on the simulation results, the optimal patterns of trajectories and signals are explored, which provide insights into the optimal traffic control actions at intersections in a cooperative vehicle environment. Furthermore, the computational performance of the proposed control approach is analyzed, and the benefits of the proposed approach on the average travel delay, throughput, fuel consumption, and emission are proved by comparing with the two-layer approaches using the car following model, the signal optimization models, and the state-of-the-art approach.

1. Introduction and motivation

Traffic lights are one of the fundamental elements on urban roads for traffic management. The red phases are beneficial to separate conflicting traffic movements at intersections, but they also cause substantial travel delay, fuel consumption and emissions on urban roads (Zhao et al., 2020). To relieve these problems, the recent advances in connected and automated vehicle (CAV) technology have attracted considerable attention. CAVs can communicate with each other and the roadside infrastructures via

Vehicle-to-Vehicle (V2V) and Vehicle-to-Infrastructure (V2I) communications (Wang et al., 2015), and consequently vehicles can be operated in an efficient, safe and sustainable way in a CAV environment, taking the real-time traffic signals into account (Feng et al., 2018). Therefore, numerous studies have investigated the cooperative design of traffic signals and/or CAV trajectories at signalized intersections taking advantage of CAV technology.

There are mainly three research directions for improving traffic operations at urban intersections using CAV technology: the classical control (e.g., signal control algorithms), guiding or controlling vehicular speeds and paths (e.g., cooperative intersection methods, speed guidance systems and CAV trajectory planning), and joint control approaches of both traffic signals and vehicle trajectories.

As to classical control, the signal control algorithms with connected vehicles (not necessarily automated vehicles) aim to generate the optimal signal parameters at an isolated intersection) (Feng et al., 2015; Chen and Sun, 2016), along a corridor (Beak et al., 2017; Li and Ban, 2018), or at the network level (Le et al., 2015; Al Islam and Hajbabaie, 2017), based on the prediction of future traffic flow states, such as vehicle speeds, arrival time and queue lengths (Guo et al., 2019a). These signal control algorithms do not optimize CAV trajectories but use connected vehicle information for state estimation and prediction. They are usually integer nonlinear programming problems and/or bi-level optimization models, which are difficult to solve. Dynamic programming (DP) (Feng et al., 2015; Chen and Sun, 2016; Beak et al., 2017; Li and Ban, 2018) and the distributed control (Le et al., 2015; Al Islam and Hajbabaie, 2017) are frequently adopted to formulate and approximate the control problems.

The cooperative intersection controller organizes the sequence of CAVs to discharge vehicles without collision at a signal-free intersection in a fully CAV environment (Lee and Park, 2012; Ahmane et al., 2013; Zohdy and Rakha, 2016; Yu et al., 2019). Vehicle trajectories before arrivals of the intersection are usually not considered in these methods. Therefore, complete and sudden stops of CAVs are sometimes inevitable in the vicinity of the intersection in order to avoid crashes, and the optimality of vehicle platooning is not guaranteed in this line of research (Yu et al., 2018). Furthermore, ignoring other road users (e.g., pedestrians, cyclists and human drivers) also challenges the realistic applications of the cooperative intersection controllers.

Individual speed guidance systems provide advisory speeds to individual vehicles for fewer vehicle stops, travel delay and/or energy consumption in the vicinity of urban intersections, such as GLOSA (Green Light Optimized Speed Advice) (Stevanovic et al., 2013; Li et al., 2014a; Stebbins et al., 2017) and Eco-Approach and Departure systems (Altan et al., 2017; Hao et al., 2018; Wang et al., 2019). The generated speed advice can also be implemented in automated vehicles, resulting in the reduction of uncertainties caused by human drivers and thereby better control performance. However, these speed guidance systems are dedicated to an individual vehicle rather than vehicle platoon(s), implying that the effects on the overall platoon or the traffic flow are ignored.

The cooperative CAV trajectory planning algorithms optimize vehicle accelerations at an isolated intersection or along a corridor, assuming that signal timings are known to the optimization models as exogenous inputs. As to the trajectory planning systems at isolated intersections, the objective functions simply consider comfort and/or fuel consumption (Jiang et al., 2017; Zhao et al., 2018; Li et al., 2018; Typaldos et al., 2020). Providing a fixed signal cycle length, the red phases at isolated intersections are normally represented as constraining the terminal conditions of vehicle position, speed and acceleration using terminal costs and/or equality constraints. These terminal conditions are normally estimated as the position of stop-line, the maximal speed and zero acceleration respectively. On the other hand, the trajectory planning systems along a corridor are usually designed for an individual vehicle such as Asadi and Vahidi (2010), Kamal et al. (2012), He et al. (2015), Wan et al. (2016) and HomChaudhuri et al. (2016), apart from the control approaches in Liu et al. (2019, 2020) which consider the overall vehicle platooning. This line of research lacks signal optimization, thus the full utilization of vehicle information (e.g., speed and position) and infrastructure information (e.g., signal timings) is hindered.

Based on previous research findings, we conclude that it is difficult to integrate traffic signal optimization with vehicle trajectory planning in a unified framework, because signal optimization and vehicle control are mutually dependent. Signals affect vehicle maneuvers and performance such as energy consumption and delay, and vehicle trajectories are of vital importance when adjusting signals in return. Therefore, the joint control approaches of traffic signals and vehicle trajectories can be solved by casting the problem in a bi-level optimization model to solve the problem iteratively (Li et al., 2014b; Yang et al., 2016; Xu et al., 2018; Feng et al., 2018; Guo et al., 2019b; Niroumand et al., 2020; Liu et al., 2021). The vehicle arrival time at the stop-line is normally required to be estimated first and then be constrained in the terminal conditions of position and speed to represent the red indication (Xu et al., 2018; Feng et al., 2018; Guo et al., 2019b; Yu et al., 2018). In the traffic signal optimization, the enumeration method (Li et al., 2014b; Xu et al., 2018; Liu et al., 2021) and the similar forward/backward recursion method (Feng et al., 2018; Guo et al., 2019b) are usually adopted to evaluate all feasible signal parameters, while signals are not explicitly optimized in Li et al. (2014b), Yang et al. (2016) and Yu et al. (2018). Furthermore, some approximation methods are adopted for relieving computational load in vehicle trajectory optimization. The rule-based trajectory patterns are designed to approximate trajectories in Li et al. (2014b) and Yang et al. (2016); the following vehicles are simulated using car following models, while only the platoon leader is controlled (Feng et al., 2018; Yu et al., 2018); each vehicle is optimized individually in Xu et al. (2018), as opposed to trajectory optimization of the overall platoon; the receding horizon scheme is adopted to update trajectories and signals (Li et al., 2014b; Yang et al., 2016; Feng et al., 2018) or update trajectories more frequently than signal timing variables (Niroumand et al., 2020), which benefits the computational load but unfortunately causes suboptimum owing to the shortsighted prediction.

This paper presents a joint control approach to simultaneously optimize traffic signals and vehicle trajectories of the overall CAV platoons in the vicinity of signalized intersections. The vehicle accelerations and signal phase lengths are jointly optimized aiming to maximize ride comfort and minimize travel delay, subject to motion constraints. The red indication is first formulated as logic constraints and then reconstructed as a series of linear position constraints. This red phase constraint formulation in our paper is generic as it requires neither the prescribed terminal conditions of speed and position nor the additional estimation of

vehicle arrival time. To further relieve the computational burden, the joint control problem is solved using mixed integer linear programming (MILP) techniques after the linearization of the objective function. The outputs of the proposed approach are the optimal signal phase lengths and the optimal acceleration trajectories of CAV platoons, thus the global optimum considering overall platoons is guaranteed within the signal cycle. This approach is scalable to incorporate multiple platoons from different movements under various traffic demand levels. To demonstrate the performance of the proposed approach, simulations under the balanced and unbalanced arrival rates from each arm are conducted, based on which the optimal vehicle trajectory pattern and the optimal traffic signal pattern are found. Finally, the comparison with the Intelligent Driver Model, the signal optimization models, and a state-of-the-art approach (Xu et al., 2018) is made, the results of which show the proposed approach generates higher throughput and less delay, energy consumption, and emission.

The contributions of this study are threefold. First, our approach simultaneously optimizes signal timing and vehicle trajectories of all platoons from multiple traffic movements. It does not require bi-level programming, nor simplifications of vehicle trajectories when optimizing signal timing, which results in nonlinear problems in general. Our formulation in mixed integer linear programming form ensures the global optimum of the control problem. Second, this paper formulates the joint problem in a single layer other than in a bi-level structure. The nonlinear formulation of this joint control problem is recast in a linear formulation, which reduces the computational load substantially. The red phases are formulated into four linear constraints, which can avoid specifying the terminal conditions of speed and position beforehand. Thereby the infeasible solutions stemming from the inaccurate arrival time estimation are bypassed. Finally, the controller performance of the proposed approach is thoroughly verified in simulation and compared with the state-of-the-art approaches, based on which the optimal signal and trajectory patterns are derived.

The rest of this paper is structured as follows. Section 2 formulates the joint optimal control problem of traffic signals and vehicle trajectories. In Section 3, the control formulation is reconstructed and linearized, followed by the introduction of the implementation approach. The controller performance is validated by simulation in Section 4, and both the optimal vehicle trajectory pattern and the optimal traffic signal pattern are explored after that, in addition to the analysis on computational performance and the comparison with the car following model, the signal optimization models, and the state of the art. Finally, conclusions and future work are delivered in Section 5.

2. Control formulation

In this section, the joint optimal control problem of traffic signals and vehicle trajectories is formulated, including problem description, specifications of control and state variables, system dynamics, the objective function and controller constraints.

2.1. Problem description

In this paper, a standard signalized intersection is considered under a given signal phase sequence. The left-turn movements are separate from the through and right-turn movements from the perspective of signal and intersection designs. The example research scenario and the predefined signal plan are illustrated in Fig. 1.

The control zone at the signalized intersection is restricted by V2V, V2I and I2V (Infrastructure-to-Vehicle) communication ranges (normally a few hundred meters), where the lane changing behavior is not considered. Vehicles in the control zone are assumed to be cooperative and thereby can be controlled via their (admissible) accelerations. Based on V2V and I2V communication, vehicle position and speed information as well as Signal Phasing and Timing (SPaT) information can be exchanged among each vehicle and the signal controller. The initial signal phase sequence is known. The sum of feedback and vehicle actuation delays is assumed to be less than 1 s and hence can be neglected in the control formulation when we choose a discrete time step size of 1 s.

The control objective is to jointly determine each signal phase length and vehicle acceleration trajectories from all traffic movements. The weighted sum of ride comfort and travel delay (i.e., a single objective function) is minimized after associating each term with a cost weight, subject to safety and physical motion constraints. The vehicle positions during the red signal indication are also constrained when optimizing signal parameters. The main variables and parameters are summarized in Table 1.

2.2. Control and state variables

The *control variables* of the joint optimal control problem are the accelerations and the signal phase switches of the signal controller, which are detailed in this subsection. The prediction horizon is the signal cycle $C \in \mathbb{Z}^+$, which is an input of the joint controller. $k \in \mathbb{Z}^+$ is the time step within the prediction horizon, and Δt is the time step size. With the choice of $\Delta t = 1$ s and $K = \frac{C}{\Delta t}$, we have $k \in \{1, 2, \dots, K\}$. Let J denote the total signal phase number within a signal cycle and j represent the signal phase sequence number, $j \in \{1, 2, \dots, J\}$. J can respond to the vehicle actuation by skipping certain phase(s) if no vehicle is detected. Hereinafter, the jth movement refers to the movement(s) which is released during the jth green phase.

If i and N^j are the vehicle sequence number and the total vehicle number in the jth movement respectively, the pair of (i, j) can thereby describe the vehicle sequence number i in the jth movement ($i \in \{1, 2, \dots, N^j\}$). N is the total vehicle number within a cycle, which can be calculated by
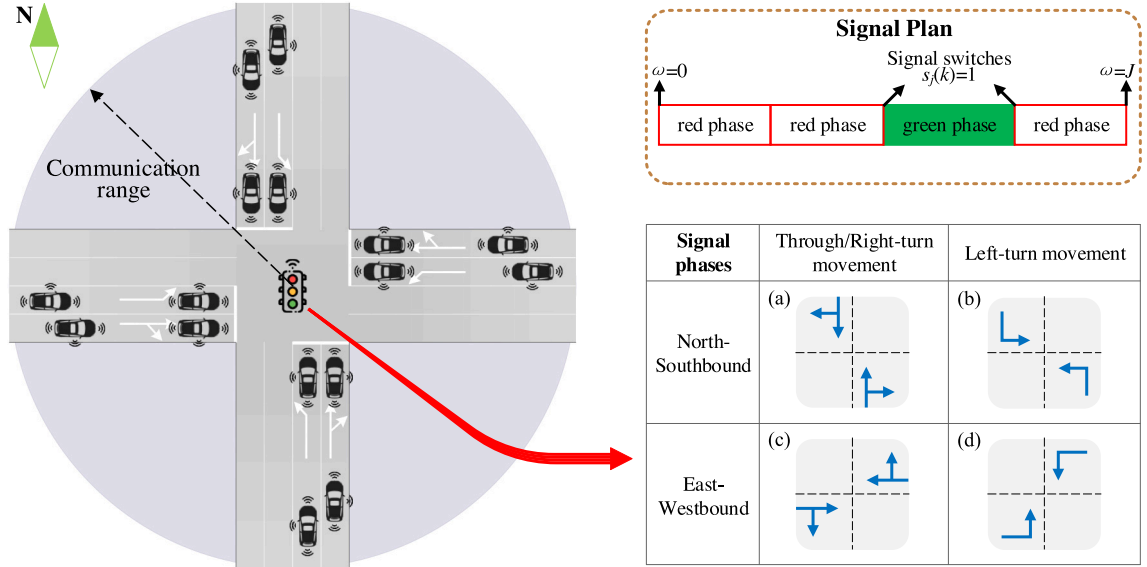
$$N = \sum_{j=1}^{J} N^j \tag{1}$$

Fig. 1. Illustration on operations of the control system.

For vehicle trajectory planning, the control variable for vehicle i in jth movement $\mathbf{u}_{ij}^V$ is acceleration (vehicle decelerations are represented as negative accelerations), as follows:

$$\mathbf{u}_{ij}^V = a_{ij}(k), k \in \{1, 2, \ldots, K\} \tag{2}$$

The state variables of the subject vehicle, $\mathbf{x}_{ij}^V$, are the longitudinal position, $x_{ij}(k)$, and the speed, $v_{ij}(k)$. The state variables of trajectory planning are

$$\mathbf{x}_{ij}^V = \begin{bmatrix} x_{ij}(k) \\ v_{ij}(k) \end{bmatrix}, k \in \{1, 2, \ldots, K\} \tag{3}$$

The control variable vector of vehicle trajectory within the signal cycle, $\mathbf{u}^V$, is defined by $\mathbf{u}_{ij}^V(k)$, as in Eq. (4). The same also holds for the state variable vector $\mathbf{x}^V$ in Eq. (5).

$$\mathbf{u}^V = \left[\underbrace{a_{11}(k), a_{12}(k), \ldots, a_{1J}(k)}_{i=1, j \in \{1,2,\ldots,J\}}, \ldots, \underbrace{a_{N^J 1}(k), a_{N^J 2}(k), \ldots, a_{N^J J}(k)}_{i=N^J, j \in \{1,2,\ldots,J\}} \right]^T, i \in \{1, 2, \ldots, N^j\}, k \in \{1, 2, \ldots, K\} \tag{4}$$

$$\mathbf{x}^V = \left[\underbrace{\mathbf{x}_{11}^T(k), \mathbf{x}_{12}^T(k), \ldots, \mathbf{x}_{1J}^T(k)}_{i=1, j \in \{1,2,\ldots,J\}}, \ldots, \underbrace{\mathbf{x}_{N^J 1}^T(k), \mathbf{x}_{N^J 2}^T(k), \ldots, \mathbf{x}_{N^J J}^T(k)}_{i=N^J, j \in \{1,2,\ldots,J\}} \right]^T, i \in \{1, 2, \ldots, N^j\}, k \in \{1, 2, \ldots, K\} \tag{5}$$

With respect to the signal optimization, the control variable is the signal state of whether or not switching the signal phase to release the jth movement at each time step, $s_j(k)$. $s_j(k)$ is defined as a binary variable, setting $s_j(k)$ equal to 1 if shifting the signal at the time step k and 0 otherwise, as shown in Eqs. (6) and (7).

$$\mathbf{u}_j^S = s_j(k), k \in \{1, 2, \ldots, K\} \tag{6}$$

$$s_j(k) = \begin{cases} 1 & \text{switching signal} \\ 0 & \text{otherwise} \end{cases} \tag{7}$$

The state variable of signal optimization is the color indication of the traffic light in the jth movement at each time step $p_j(k)$. $p_j(k) = 1$ if the signal controller indicates red and otherwise $p_j(k) = 0$, as can be seen in Eqs. (8) and (9).

$$\mathbf{x}_j^S = p_j(k), k \in \{1, 2, \ldots, K\} \tag{8}$$

$$p_j(k) = \begin{cases} 1 & \text{red signal indication} \\ 0 & \text{green signal indication} \end{cases} \tag{9}$$

Table 1
List of notations.

General variables and parameters	
$\mathbb{R}$	Set of real numbers
$\mathbb{Z}$	Set of integers
$\mathbb{Z}^+$	Set of positive integers
$C \in \mathbb{Z}^+$	Signal cycle length, s
$\Delta t = 1$	Time step size, s
$K = \frac{C}{\Delta t} \in \mathbb{Z}^+$	Total number of time steps, i.e., prediction horizon
$k \in \mathbb{Z}^+$	Time index, $k \in \{1, 2, \ldots, K\}$
$J \in \mathbb{Z}^+$	Total number of signal phases in a signal cycle
$j \in \mathbb{Z}^+$	Sequence number of signal phase, $j \in \{1, 2, \ldots, J\}$
$\omega \in \mathbb{Z}^+$	Sequence number of phase start/end (signal switch) in a signal cycle, $\omega \in \{0, 1, \ldots, J\}$
t_ω	The moment of the ωth signal switch, s
$N^j \in \mathbb{Z}^+$	Vehicle number in the jth movement
$N \in \mathbb{Z}^+$	Total vehicle number in a signal cycle
(i, j)	Vehicle sequence number i in the jth movement
β_1, β_2	Cost weights
H	Objective function
M	A large value
$A^j(\omega)$	Attached moment of signal switch, s
l_{ij}	The length of the ith vehicle in the jth movement, m
x_{stop}^j	Longitudinal position of the stop-line regarding the jth movement, m
$a_{\min}$	The minimal acceleration, m/s^2
$a_{\max}$	The maximal acceleration, m/s^2
$v_{\max}$	The maximal speed, m/s
$t_{\min}$	The minimum safe car-following time gap, s
s_0	The minimum space gap at standstill conditions, m
$T_m^{\max}$	Maximal number of the released traffic movements
T_m	Released traffic movement sequence, $T_m \leqslant T_m^{\max}$
P_j	The jth optimal signal phase length, s
f_{eco}	The instantaneous fuel consumption rate, ml/s
Control variables	
$a_{ij}(k)$	Discrete control variable, acceleration of the ith vehicle in the jth movement
$s_j(k)$	Discrete control variable, signal switch in the jth movement
$\gamma_{ij}(\omega)$	Auxiliary control variable, binary variable of passing the intersection or not at the moment of the ωth signal switch
$q_{ij}(k)$	Auxiliary control variable for linearization
$r_{ij}(k)$	Auxiliary control variable for linearization
$\mathbf{u}^V$	Control variable vector of vehicle trajectory optimization for all vehicles in all movements
$\mathbf{u}^S$	Control variable vector of traffic signal optimization for all vehicles in all movements
$\mathbf{u}$	Control variable vector of the joint controller for all vehicles in all movements
Γ	Control variable vector of $\gamma_{ij}(\omega)$ for all vehicles in all movements
State variables	
$x_{ij}(k)$	Discrete state variable, position of the ith vehicle in the jth movement
$v_{ij}(k)$	Discrete state variable, speed of the ith vehicle in the jth movement
$p_j(k)$	State variable, binary variable of traffic signal indication in the jth movement
$\mathbf{x}^V$	State variable vector of vehicle trajectory optimization for all vehicles in all movements
$\mathbf{x}^S$	State variable vector of signal optimization for all vehicles in all movements

The control and state variable vectors of signal optimization regarding all traffic movements within the cycle, $\mathbf{u}^S$ and $\mathbf{x}^S$, are defined by $\mathbf{u}_j^S(k)$ and $\mathbf{x}_j^S(k)$ in time ($k \in \{1, 2, \ldots, K\}$, $j \in \{1, 2, \ldots, J\}$). It is also noted that the control variable vector of the joint controller is defined by $\mathbf{u}^V$ and $\mathbf{u}^S$, thus

$$\mathbf{u} = \begin{bmatrix} \mathbf{u}^V \\ \mathbf{u}^S \end{bmatrix} \tag{10}$$

2.3. System dynamics

The system dynamics model of the joint optimal control problem is presented separately for trajectory planning (as Eq. (11) and signal optimization (in Eq. (12)). For the trajectory optimization subproblem, the system dynamics model is described using the following second-order equation.

$$\mathbf{x}_{ij}^V(k+1) = A\mathbf{x}_{ij}^V(k) + B\mathbf{u}_{ij}^V(k) \tag{11}$$

where

$$A = \begin{bmatrix} 1 & \Delta t \\ 0 & 1 \end{bmatrix}; B = \begin{bmatrix} \frac{1}{2}\Delta t^2 \\ \Delta t \end{bmatrix}$$

Here, Δt denotes the time step size. In addition, the dynamics equation of signal optimization is

$$p_j(k+1) = \left| p_j(k) - s_j(k) \right| \tag{12}$$

2.4. Objective function

Within the prediction horizon ($k \in \{1, 2, \ldots, K\}$), the ride comfort and travel delay of all controlled vehicles from all traffic movements are taken into account by minimizing the absolute value of accelerations and maximizing speeds. The objective function is designed as follows:

$$H = \min_{\mathbf{u}} \sum_{j=1}^{J} \sum_{i=1}^{N^j} \sum_{k=1}^{K} [\beta_1 |a_{ij}(k)| - \beta_2 v_{ij}(k)] \tag{13}$$

Here, β_1 and β_2 are cost weights. The unit of β_1 is defined as second and β_2 is unitless. The first cost term of ride comfort is designed to reduce fluctuations in accelerations. The second cost term of travel delay aims at stimulating vehicles to speed up, departing the intersection as soon as possible.

2.5. Controller constraints

The joint optimal controller requires the control and state variables to respect certain constraints, i.e., admissible accelerations, maximum speed bounds, safe driving requirements, signal switch limitation and the red phase position constraints.

For vehicle trajectory planning, the accelerations of all vehicles are bounded within the admissible range between the maximal acceleration, $a_{\max}$, and the minimal acceleration (i.e., the negative of the maximal deceleration), $a_{\min}$.

$$a_{\min} \leq a_{ij}(k) \leq a_{\max} \tag{14}$$

The speeds of all vehicles are restricted to be positive but not larger than the limit speed, $v_{\max}$.

$$0 \leq v_{ij}(k) \leq v_{\max} \tag{15}$$

As to the safe driving requirements, the following vehicles should keep at least the minimal safe gap with the vehicles in front. If l_{ij} denotes the length of vehicle i in the jth movement, $t_{\min}$ is the minimum safe car-following time gap, and s_0 is the minimum space gap at standstill conditions, the safety requirements can be represented as:

$$x_{i-1,j}(k) - x_{ij}(k) - v_{ij}(k)t_{\min} - s_0 - l_{ij} \geq 0, i \geq 2 \tag{16}$$

In terms of signal optimization, the signal cycle is supposed to contain at least a green phase and a red phase for each traffic movement, thus the signal indication should switch at most twice within the prediction horizon. The total signal switch number of the jth movement is constrained as follows.

$$\sum_{k=1}^{K} s_j(k) \leq 2 \tag{17}$$

Vehicles are required to respond to signal changes when jointly optimizing traffic signals and vehicle trajectories. In order to connect vehicle positions with signal indications, auxiliary variables are introduced to represent the red phases. Let ω ($\in \{0, 1, \ldots, J\}$) denote the sequence number of phase start/end (i.e., the signal switch), as illustrated in Fig. 1 where $\omega = 0$ refers to the beginning of the signal cycle and $\omega = J$ is the signal cycle tail. Furthermore, the auxiliary binary variable of vehicle position condition, $\gamma_{ij}(\omega)$, is introduced to represent whether or not the ith vehicle in the jth movement can pass the intersection when switching the ωth signal. At the specific moment of the ωth signal switch, $\gamma_{ij}(\omega)$ is defined as 1 if the subject vehicle cannot pass, and $\gamma_{ij}(\omega) = 0$ if it can pass the stop-line. To reflect the ωth signal switch in time, we refer to t_ω as the time step of the ωth traffic signal switch, i.e., the time when the $(\omega+1)$th signal phase starts. Therefore, vehicle position condition $\gamma_{ij}(\omega)$ is represented using state variables of $x_{ij}(t_\omega)$ and $p_j(t_\omega)$, as follows.

$$\gamma_{ij}(\omega) = \begin{cases} 1 & x_{ij}(t_\omega) \leq 0 \\ 0 & \text{otherwise} \end{cases}, p_j(t_\omega - 1) \neq p_j(t_\omega), \omega \in \{0, 1, \ldots, J\} \tag{18}$$

In the joint optimization of signals and trajectories, the vehicle position conditions $\gamma_{ij}(\omega)$ are known at the beginning and the tail of the signal cycle (i.e., $\omega = 0$ and $\omega = J$), but unknown at the intermediate signal switches when $\omega \in \{1, 2, \ldots, J-1\}$. Nevertheless, the unknown intermediate $\gamma_{ij}(\omega)$ values can be exploited using the known position conditions $\gamma_{ij}(0)$ and $\gamma_{ij}(J)$, because the vehicle position condition remains constant during any red phase, either behind or beyond the stop-bar. Therefore, the red phase expression of Eq. (18) is recast into Eq. (19), the idea of which is to convert the known position condition values to the uncertain position conditions when switching the ωth ($\in \{1, 2, \ldots, J-1\}$) signal.

$$\gamma_{ij}(\omega) = \begin{cases} \gamma_{ij}(0) & , \text{if } p_j(t_\omega - 1) = 1 \ \& \ p_j(t_\omega) = 0 \\ \gamma_{ij}(K) & , \text{if } p_j(t_\omega - 1) = 0 \ \& \ p_j(t_\omega) = 1 \end{cases}, \omega \in \{1, 2, \ldots, J-1\} \tag{19}$$

As shown in Eq. (19), $\gamma_{ij}(\omega) = \gamma_{ij}(0)$ if the ωth signal switches to the green phase, and $\gamma_{ij}(\omega) = \gamma_{ij}(K)$ if the ωth signal switches to the red phase in the current signal cycle. In this way, the red phase design is represented using the logic constraints of Eqs. (18) and (19).
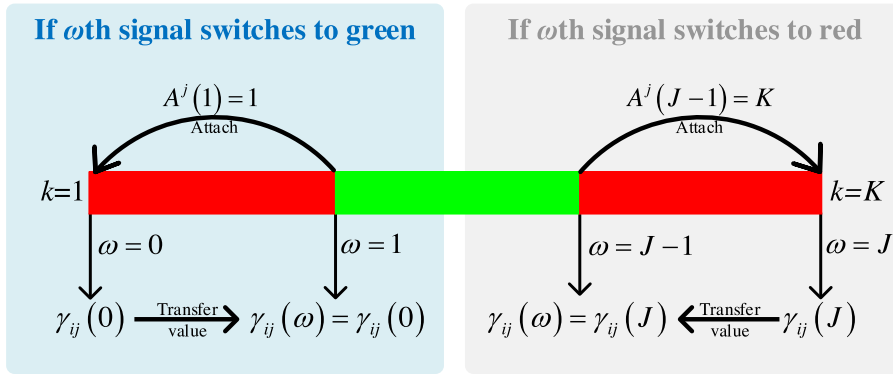
Fig. 2. Illustration of signal switches and attached moments.

3. Solution approach

The dimension of the joint control problem can be significantly large under high traffic demand levels. In order to relieve the excessive computational load, the control formulation presented in Section 2 is reconstructed in this section. The red phase representation using logic constraints of Eqs. (18) and (19) is first linearized, followed by linearization of the objective function. Finally, the implementation approach is introduced.

3.1. Linear formulation of red phase constraints

The red phase representation of Eqs. (18) and (19) are logic constraints, which are difficult to solve. To bypass this issue, the auxiliary variable of vehicle position condition $\gamma_{ij}(\omega)$ is introduced as additional control variable. If Γ is defined by $\gamma_{ij}(\omega)$ (see Eq. (20)), the control variable vector of the joint controller is replaced by Eq. (21).

$$\Gamma = [\underbrace{\gamma_{11}(1),\ldots,\gamma_{1J}(1)}_{\omega=1},\ldots,\underbrace{\gamma_{11}(J-1),\ldots,\gamma_{1J}(J-1)}_{\omega=J-1},\ldots,\underbrace{\gamma_{NJ1}(1),\ldots,\gamma_{NJJ}(1)}_{\omega=1},\ldots,\underbrace{\gamma_{NJ1}(J-1),\ldots,\gamma_{NJJ}(J-1)}_{\omega=J-1}]^T \tag{20}$$

$$\underbrace{\qquad\qquad}_{i=1, j\in\{1,2,\ldots,J\}} \qquad\qquad \underbrace{\qquad\qquad}_{i=NJ, j\in\{1,2,\ldots,J\}}$$

$$\mathbf{u} = \begin{bmatrix} \mathbf{u}^S \\ \mathbf{u}^V \\ \Gamma \end{bmatrix} \tag{21}$$

The problem arises when representing the additional system dynamics of the position condition $\gamma_{ij}(\omega)$, owing to its logical and binary features. However, the relationship between the position condition and the original control and state variables can be described as a series of inequality equations, as discussed below.

Although the phase lengths are jointly optimized and thereby unknown in the control formulation, $\gamma_{ij}(\omega)$ stays unchanged within the red signal indication, as discussed previously. Hereinafter, the red phase logic constraints of Eqs. (18) and (19) are reformulated by introducing the piecewise time moment $A^j(\omega)$ ($\omega \in \{1, 2, \ldots, J-1\}$). $A^j(\omega)$ is designed to attach the moment of the certain signal switch to the beginning or the end of the signal cycle ($k = 1, K$), as in Eq. (22). The illustration of the signal switch and the attached moment $A^j(\omega)$ within a signal cycle are explained in Fig. 2. The first (or the second) red time can be removed if the signal cycle starts (or ends) with the green phase. In Eq. (22), the attached moment equals to the time step of either the beginning or the end of the current cycle, i.e., $A^j(\omega) = 1$ if the ωth signal switches to the green phase and $A^j(\omega) = K$ otherwise.

$$A^j(\omega) = \begin{cases} 1 & p_j(t_\omega - 1) = 1, p_j(t_\omega) = 0 \\ K & p_j(t_\omega - 1) = 0, p_j(t_\omega) = 1 \end{cases}, \omega \in \{1, 2, \ldots, J-1\} \tag{22}$$

Furthermore, four linear constraints of Eq. (23) to Eq. (26) are proposed to restrict vehicle positions during the red phase(s) without specific signal parameters. Let x_{stop}^j imply the longitudinal position of the stop-bar in the jth movement, and M is a large value. Under the workings of these four constraints, the known position condition values can be transferred from the beginning/end of the signal cycle to the unspecific moments of signal switches.

The constraints of Eqs. (23) and (24) demonstrate the position condition at the ωth signal switch equal to the position condition at the attached moment (either the beginning or the end of the signal cycle). Taking Fig. 2 as an example, if the vehicle can pass the intersection during the green phase ($\gamma_{ij}(J-1) = 0$), Eqs. (23) and (24) require the vehicle position to be larger than or equal to the position of the stop-bar at the end of the current signal cycle, $x_{ij}(A^j(J)) \geq x_{\text{stop}}^j$. Similarly, the terminal position condition of stopping vehicles that cannot depart the intersection ($x_{ij}(K) \leq x_{\text{stop}}^j, \gamma_{ij}(J) = 1$) is also conveyed to the $(J-1)$th signal switch via $A^j(\omega)$, thus $\gamma_{ij}(J-1) = 1$. If the subject vehicle is behind the stop-bar at the beginning of the signal cycle, i.e., $\gamma_{ij}(0) = 1$, this

position condition is transferred to the first signal switch by the attached moment, thus $\gamma_{ij}(1) = 1$. In this way, the vehicle position remains unchanged during the red phase(s) in the signal cycle under indefinite signal parameters.

$$x_{ij}(A^j(\omega)) - x_{\text{stop}}^j \leq (1 - \gamma_{ij}(\omega))M \tag{23}$$

$$-x_{ij}(A^j(\omega)) + x_{\text{stop}}^j \leq \gamma_{ij}(\omega)M \tag{24}$$

Regarding the remaining time within the signal cycle, the vehicle position constraints are elaborated in Eqs. (25) and (26). As denoted above, t_ω is the time step of the ωth signal switch, thus $s_j(t_\omega) = 1$ means that the traffic signal is switched at $t = t_\omega$ and otherwise $s_j(t_\omega) = 0$. Therefore, the position condition $\gamma_{ij}(\omega)$ is unchanged until the traffic signal is switched (i.e., $s_j(t_\omega) = 1$).

$$x_{ij}(k) - x_{\text{stop}}^j \leq (1 - \gamma_{ij}(\omega))M + (1 - s_j(t_\omega))M \tag{25}$$

$$x_{ij}(k) - x_{\text{stop}}^j \geq -\gamma_{ij}(\omega)M - (1 - s_j(t_\omega))M \tag{26}$$

In this way, the red phase logic constraints of Eqs. (18) and (19) are replaced by a series of linear constraints.

3.2. Linearization of the objective function

To simplify this control formulation, the first cost term in the objective function of Eq. (13) should be linearized. Two auxiliary non-negative variables $q_{ij}(k)$ and $r_{ij}(k)$ are introduced as follows:

$$q_{ij}(k) = \frac{|a_{ij}(k)| + a_{ij}(k)}{2}, q_{ij}(k) \geq 0 \tag{27}$$

$$r_{ij}(k) = \frac{|a_{ij}(k)| - a_{ij}(k)}{2}, r_{ij}(k) \geq 0 \tag{28}$$

Therefore, the accelerations and the ride comfort cost term can be represented as

$$a_{ij}(k) = q_{ij}(k) - r_{ij}(k), q_{ij}(k) \geq 0, r_{ij}(k) \geq 0 \tag{29}$$

$$|a_{ij}(k)| = q_{ij}(k) + r_{ij}(k), q_{ij}(k) \geq 0, r_{ij}(k) \geq 0 \tag{30}$$

The auxiliary variables of $q_{ij}(k)$ and $r_{ij}(k)$ can be regarded as additional control variables in the controller, subject to the above linear equality constraints. Replace the ride comfort cost term in the objective function using Eq. (30), then the control problem is reformulated as:

$$H = \min_{\mathbf{u}} \sum_{j=1}^{J} \sum_{i=1}^{N^j} \sum_{k=1}^{K} [\beta_1(q_{ij}(k) + r_{ij}(k)) - \beta_2 v_{ij}(k)] \tag{31}$$

subject to constraints of Eqs. (11), (12), (14) to (17), (23) to (26), and (29).

3.3. Implementation

The control variables contain integer variables of signal state $s_j(k)$ and position condition $\gamma_{ij}(\omega)$, so the optimal control problem can be solved using mixed integer linear programming (MILP) techniques. The system dynamics of Eqs. (11) and (12) and the linearization equation via auxiliary variables Eq. (29) are implemented as linear equality constraints. The state variables of speeds and positions can be represented using accelerations via the system dynamic equation. Therefore, all linear inequality constraints of Eqs. (14) to (17) and (23) to (26) are transformed to restrict the control variable acceleration. This optimal control problem is solved using intlinprog solver in MATLAB.

To be noted, the optimization solver intlinprog is warm-started to expedite the runtime. The initial guess of the signal plan is assumed to divide the signal cycle evenly into average signal phases. The initial guess of accelerations is the maximal acceleration until reaching the maximal speed at the beginning of green phases. The initial guess of position condition $\gamma_{ij}(\omega)$ is estimated by the vehicle positions at the end of green phases under the initial acceleration guess, i.e., whether the vehicles can pass the intersection. The joint optimal control algorithm yields the optimal signal parameters and the optimal vehicle trajectories. In the forthcoming section, the outputs of this control algorithm are presented and analyzed before the optimal patterns of trajectories and signals are explored.

4. Simulation results and analysis

In order to demonstrate the performance of this controller, the simulation results are discussed after designing several experiments in this section. The optimal results have the single optimum due to the linearity feature of the control formulation.

Table 2
Procedure of tuning cost weights.

Value of β_1	Value of β_2	Results
1	1	Accelerations fluctuate dramatically at the end of the green phases.
3	1	There are unnecessary fluctuations in accelerations facing the red phases.
5	1	Few vehicles perform unsmooth accelerations.
7	1	Accelerations and speeds are smooth, and most vehicles can reach the maximal speed after the green phases.

4.1. Experiment design

Multiple simulation experiments are designed to validate the performance of the control algorithm, taking into account the overall controlled vehicle numbers N, the maximal numbers of the released traffic movements $T_m^{\max}$ (corresponding to each arm during every signal phase), and the signal cycle lengths C. The overall controlled vehicles include the queuing vehicles at the stop-line and the approaching vehicles from the boundary of the control zone. To verify the flexibility of the joint control approach in incorporating various signal designs, the controlled vehicles are released into multiple movements under $T_m^{\max} = 4, 6, 8$ within the cycle lengths from 40 s to 60 s respectively. When $T_m^{\max} = 4$, the turning movements are indistinct at the intersection, thus the traffic movements of (a) and (b) (see Fig. 1) are regarded as two movements from two opposite arms which are released during the first phase, and movements of (c) and (d) are released during the other phase. When $T_m^{\max} = 6$, the turning movements from one pair of the two opposite arms (either movements of (a) and (b) in the northbound/southbound direction or movements of (c) and (d) in the eastbound/westbound direction) are not differentiated at the intersection, which means they are released together in one green phase. The remaining movements of (c) and (d) (or (a) and (b)) are discharged separately during two green phases with the distinction of left-turning movements. When $T_m^{\max} = 8$, traffic movements (a) to (d) depart the intersection in sequence respectively within four signal phases. To be noted, the signal phase(s) can be skipped based on the vehicle actuation if no queuing and incoming vehicles are detected. In other words, the signal phase number J is optimized based on the released traffic movements. Hereinafter, the released traffic movement sequence is denoted by T_m ($\leqslant T_m^{\max}$), and thereby the jth signal phase discharges the traffic movements of $T_m = j, j + J$ from two opposite arms, if no signal phase is skipped.

Different objectives are weighted in a linear way to select appropriate cost weight values according to the posteriori method. When the other cost weight is constant, the magnitude of ride comfort cost weight β_1 affects the fluctuations of accelerations. Smaller values of β_1 result in more frequent variations on accelerations, while vehicles may not reach the maximal speed if β_1 is overweighted, causing lower traffic efficiencies because of unable to fully utilize the green phases. The cost weights of β_1 and β_2 are tuned based on the scenario with the largest dimension of control variables, and then applied in all scenarios. First, β_2 is fixed to be 1, and then β_1 is increased from 1 until the variations of accelerations/decelerations are smooth facing the red phases and most vehicles can reach the maximal speed after the green phase. Finally, β_1 is selected to be 7 when $\beta_2 = 1$, the acceleration trajectories under which are smooth without any unnecessary fluctuation, and the vehicle speeds are able to reach the maximal speed passing the intersection. The procedure of tuning cost weights is summarized in Table 2. Similar controller tuning can be found in (Lee and Yu, 1994; Burger et al., 2013; Liu et al., 2020; Zhao et al., 2020; Liu et al., 2021).

The parameter and coefficient values are detailed in Table 3, which mainly come from our previous work (Liu et al., 2020). The designed initial conditions in Table 3 are representative. In addition, similar settings and initial conditions add no difficulty on implementation. Delays under 1 s can be ignored because the time step is 1 s.

4.2. Operational performance analysis

To verify the feasibility of the control algorithm, the performance of the proposed approach is simulated under different traffic demand levels, signal cycle lengths and the maximal released traffic movement numbers, as detailed in Table 4. First, the controller performance is explored thoroughly under the balanced vehicle arrival rates from different arms, i.e., the uniform vehicle settings of Case 1, 2 and 3 per movement released into at most 4, 6 and 8 traffic movements ($T_m^{\max} = 4, 6, 8$) within the cycle lengths from 40 s to 60 s. For concise demonstration, only two scenarios under the balanced vehicle arrival rates are selected to present the optimal trajectories and the optimal signals (Scenario 1 and 2). In addition, Scenario 3 and 4 are designed under the unbalanced vehicle arrival rates from each arm considering the signal phase sequences and turning proportions. The objectives of Scenario 1 to Scenario 4 aim to not only explore the controller performance of the optimal trajectories when platoons react to the optimal signals, but prove the feasibility of the proposed approach in integrating the oversaturated traffic flow and the balanced/unbalanced arrival rates, considering various signal plans and turning proportions under different cycle lengths and the maximal released movements.

The traffic demand levels and the vehicle arrival rates under all scenarios are detailed as follows. The total controlled vehicle numbers are different under four scenarios in order to test the performance of the proposed approach under various traffic demand levels, such as in Scenario 2 and 4 where the controlled vehicle numbers are larger than the maximal vehicle numbers to be released while fewer vehicles are included in Scenario 1 and 3. The controlled vehicle numbers of each movement are balanced in Scenario 1 and 2, i.e., 4 queuing vehicles at the stop-bar and 4 approaching vehicles from the upstream direction of the intersection (referring to Case 3). However, the vehicle arrival rates from each arm are unbalanced in Scenario 3 and 4, which means the compositions of the queuing and approaching vehicle platoons from 8 movements are randomly generated, just like determining the number of balls in each basket when throwing N balls into 16 baskets randomly.

Table 3

Parameter and coefficient values.

Notation	Parameter/ Coefficient	Value	Unit
–	Initial speed of approaching vehicles	10	m/s
–	Initial space gap of approaching vehicles	25	m
–	Initial position of the leader in the approaching vehicles	−200	m
–	Initial space gap of queuing vehicles	5	m
–	Initial position of the leader in the queuing vehicles	−5	m
–	Control zone range	200	m
Δt	Time step size	1	s
M	A large value	100000	–
l_{ij}	Length of the ith vehicle in the jth movement	3	m
x_{stop}^j	Position of the stop line	0	m
$a_{\min}$	Allowable minimum acceleration	−5	m/s^2
$a_{\max}$	Allowable maximum acceleration	2	m/s^2
$v_{\max}$	Limit speed	20	m/s
$t_{\min}$	Minimum safe car-following time gap for the right-turn, through and left-turn movements respectively	3,2,2.5	s
s_0	Minimum space gap at standstill conditions	2	m
β_1	Cost weight	7	s
β_2	Cost weight	1	–
–	Queueing vehicle number per movement in Case 1, 2, 3	2, 3, 4	–
–	Approaching vehicle number per movement in Case 1, 2, 3	2, 3, 4	–
N^j	Total vehicle number per movement in Case 1, 2, 3	4, 6, 8	–
$T_m^{\max}$	Maximal number of the released traffic movements within the signal cycle	4, 6, 8	–
C	Signal cycle length	40, 41, …,60	s

Table 4

Scenario design.

Scenario design	Scenario 1	Scenario 2	Scenario 3	Scenario 4
Cycle length (s)	$C = 50$	$C = 60$	$C = 50$	$C = 40$
Maximal released movements	$T_m^{\max} = 6$	$T_m^{\max} = 8$	$T_m^{\max} = 8$	$T_m^{\max} = 8$
Total controlled vehicle number (veh/cycle)	$N = 48$	$N = 64$	$N = 44$	$N = 48$
Maximal vehicle number to be released (veh/cycle)	50	60	50	40
Controlled vehicle number per movement (veh/movement)	8 veh/movement of Case 3 (4 queuing and 4 approaching veh)	8 veh/movement of Case 3 (4 queuing and 4 approaching veh)	Randomly generated	Randomly generated
Vehicle arrival rates per movement	Balanced	Balanced	Unbalanced	Unbalanced
Signal phase sequence	–	–	Left-turn movement is released first	Left-turn movement is released afterwards
Turning proportions of the right-turn movements	–	–	0.3, 0.3, 0.3, 0.3	0.3, 0.4, 0.5, 0.6

The turning movements and signal designs under all scenarios are hereinafter disclosed. Scenario 1 and 2 do not distinguish the turning movements, and thereby the desired time headways are 2 s for all vehicles. However, the movements of right turning, through and left turning can be reflected by adopting different values of the minimal safe car-following time gap $t_{\min}$ (see Table 3). Scenario 3 and 4 make a distinction between the different signal phase sequences and the turning proportions. In Scenario 3, the left-turn movements ($T_m = 1, 3, 5, 7$) are released prior to the through/right-turn movements ($T_m = 2, 4, 6, 8$), while things are opposite under Scenario 4. The left-turn movements have exclusive lanes and signal phases, thus the left-turn proportions are equal to 1. For the through/right-turn shared movements, the right-turn proportions in movements of $T_m = 2, 4, 6, 8$ are 0.3 under Scenario 3, while the right-turn proportions under Scenario 4 are 0.3, 0.4, 0.5 and 0.6 in movements of $T_m = 1, 3, 5, 7$ respectively. In addition, the vehicle compositions of through and right-turn vehicles in the through/right-turn shared movements are produced at random.

In general, the simulation results of Scenario 1 to Scenario 4 show that vehicles are able to respond to the optimal signals via smooth trajectories and all constraints are satisfied. The passing vehicles reach the maximal speed as soon as possible and the stopping vehicles perform to decelerate from the initial speed, smoothly approaching the stop-line with lower speeds. When the green phase starts, vehicles behind the stop-bar accelerate to pass but still keep the safe following gaps with the vehicles in front. It can be concluded that the control approach is feasible under different traffic demand levels, vehicle arrival rates and signal designs. In addition, the joint controller is flexible in accounting for multiple platoons from various traffic turning movements, including queuing and approaching vehicles at the intersection. The optimal trajectories under Scenario 1 to Scenario 4 and the optimal signals are explored and discussed below.
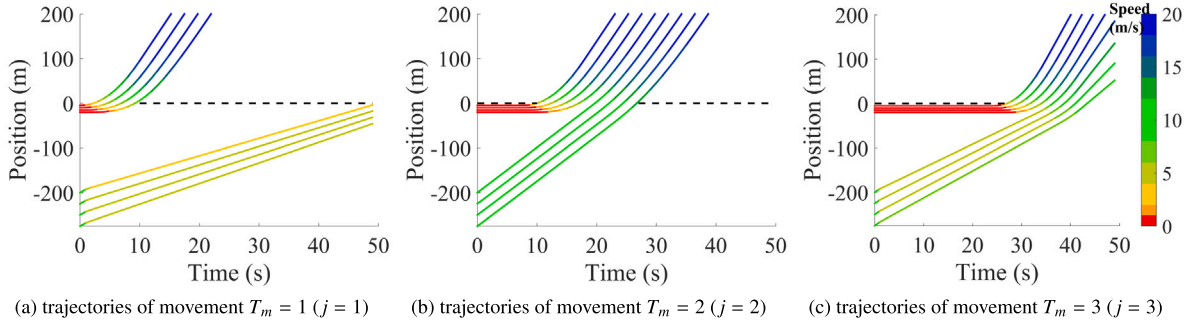
(a) trajectories of movement $T_m = 1$ ($j = 1$)   (b) trajectories of movement $T_m = 2$ ($j = 2$)   (c) trajectories of movement $T_m = 3$ ($j = 3$)

Fig. 3. Optimal performance under Scenario 1.

4.2.1. Vehicle trajectory pattern

The optimal performance of longitudinal position trajectories under all scenarios are depicted in Figs. 3 to 6. In Figs. 3 and 4, the trajectories of movements $T_m = 5, 6, 7, 8$ are not presented under Scenario 1 and 2, because they are the same as the trajectories of movements $T_m = 1, 2, 3, 4$ under the balanced vehicle arrival rates. Other scenarios of the balanced vehicle arrival rates that are not presented here have the significantly similar performance as Scenario 1 and 2. The optimal red phase lengths are depicted as black dashed lines at the stop-bar in these figures, and the vehicle sequence number in the legend of Fig. 4(h) starts from the queuing vehicle with the largest initial position (Vehicle 1) to the approaching vehicle in the platoon tail.

The trajectories under all scenarios demonstrate that all vehicles are able to react to the signal changes, as the longitudinal position subfigures in Figs. 3 to 6. Thus, the red phase constraints of Eqs. (23) to (26) are proved to be effective in the joint control formulation. In addition, typical vehicle trajectories such as accelerations/decelerations of stopping, passing and queuing vehicles are considerably smooth, as can be seen in the acceleration subfigures of Fig. 4(e) to (h).

The optimal trajectory pattern of vehicles' approach/exit, acceleration, merge, and platoon stability can be summarized from the optimal performance under all scenarios in Figs. 3 to 6. Vehicles tend to avoid stops and try to exit the intersection at higher speeds. At the beginning of the green phase, the queuing vehicles accelerate dramatically from the stationary condition, aiming to exit the intersection as soon as possible. This acceleration pattern of queuing vehicles is evident when we look at the accelerations of Vehicle 1 in Fig. 4. When merging, vehicles may decrease the acceleration rates a little bit to keep the safe gap with the preceding vehicles. With respect to the acceleration fluctuations, the following vehicles always perform smaller changes than the predecessors, which proves the platoon stability.

In Scenario 3 and 4, the turning movements are distinguished using the minimal safe car-following time gap $t_{\min}$, i.e., setting $t_{\min} = 3$ s for the right-turn movement, $t_{\min} = 2$ s for the through movement and $t_{\min} = 2.5$ s for the left-turn movement. The turning movements are depicted as the solid lines for the through movement, the dotted lines for the right-turn movement and the dashed lines for the left-turn movement in Figs. 3 to 6. The differences in the gaps between the right-turn and through movements are obvious (see the second and third vehicles in Fig. 5(b), for instance). The optimal trajectory pattern is still respected under Scenario 3 and 4 considering various turning proportions and signal phase sequences, as can be seen in Figs. 3 to 6. Therefore, the flexibility of the proposed control approach in incorporating different signal designs and turning movements is verified.

Furthermore, the approaching vehicles in the movements of $T_m = 4, 8$ confront a long preceding red phase, so they have to decelerate and arrive at the stop-line with relatively low speeds. For instance, the arrival speeds of approaching vehicles in movements of $T_m = 2$ and 4 are normally 12 m/s and 4 to 5 m/s respectively. Therefore, the traffic efficiency of releasing vehicles in movements of $T_m = 4$ and $T_m = 8$ is lower compared to the other movements, which is demonstrated by the dispersion in position trajectories during the green phases in the movements of $T_m = 4$ and 8, as can be seen in Figs. 3(c), 4(d), 5(d) and (h), 6(d) and (h). This lower efficiency in the movements of $T_m = 4$ and 8 also affects the performance of the optimal signals, which will be detailed in the discussion of the traffic signal pattern.

4.2.2. Traffic signal pattern

In order to explore the signal pattern, the optimal signals under the balanced vehicle arrival rates of Case 1, 2, and 3 with the cycle lengths from 40 s to 60 s are listed, as in Table 5 ($T_m^{\max} = 6$) and Table 6 ($T_m^{\max} = 8$). Furthermore, the optimal signals under the cycle lengths of 40 s, 50 s, and 60 s are presented in Fig. 7 for convenience of analysis, where the signal phase lengths are arranged in sequence. If P_j denotes the length of the jth signal phase, the green, gray, red and blue lines in Fig. 7 represent the first phase length P_1 to the last phase length P_4 respectively. Again, the movements of $T_m = 5, 6, 7, 8$ under the balanced vehicle arrival rates are omitted.

The signals are optimized to release as many vehicles as possible by switching signal phases in time, owing to the travel delay cost term in the objective function of Eq. (31). The benchmark values observed from the optimal signals are identified for analysis, that is, releasing all vehicles as soon as possible in P_1 under Case 1, 2 and 3 requires 14 s, 16 s and 20 s respectively, and the counterparts in P_2 are 8 s, 12 s and 17 s. Hereinafter, the oversaturated traffic flow represents the situation that some vehicles have to be left within the signal cycle. The undersaturated traffic flow refers to the condition that all vehicles can be released within
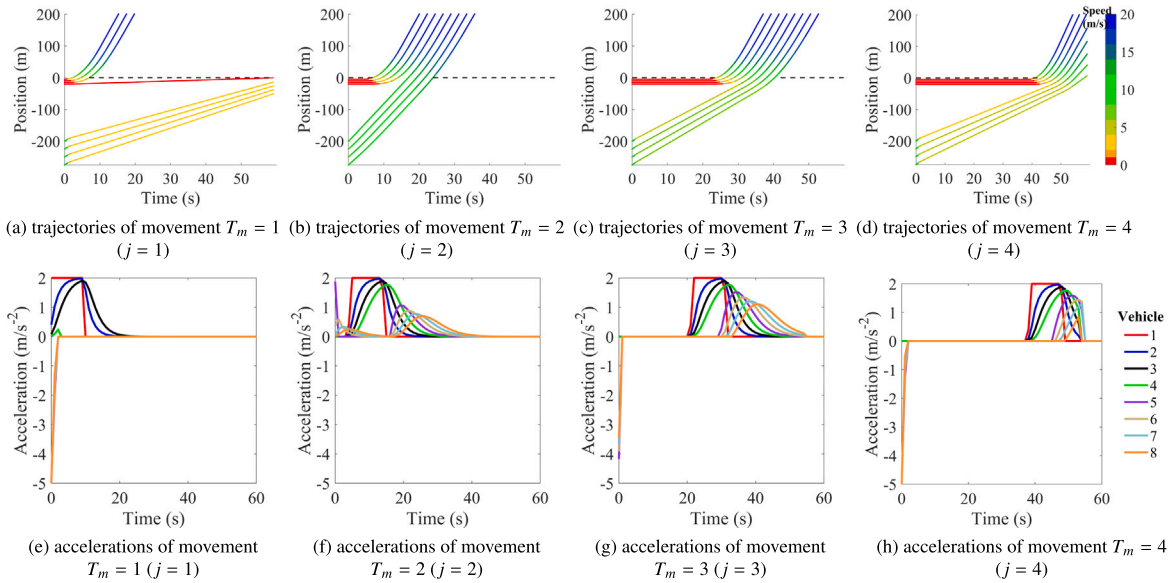
(a) trajectories of movement $T_m = 1$ (b) trajectories of movement $T_m = 2$ (c) trajectories of movement $T_m = 3$ (d) trajectories of movement $T_m = 4$
($j = 1$)   ($j = 2$)   ($j = 3$)   ($j = 4$)

(e) accelerations of movement (f) accelerations of movement (g) accelerations of movement (h) accelerations of movement $T_m = 4$
$T_m = 1$ ($j = 1$) $T_m = 2$ ($j = 2$) $T_m = 3$ ($j = 3$)   ($j = 4$)

Fig. 4. Optimal performance under Scenario 2.

(a) trajectories of movement $T_m = 1$ (b) trajectories of movement $T_m = 2$ (c) trajectories of movement $T_m = 3$ (d) trajectories of movement $T_m = 4$
($j = 1$)   ($j = 2$)   ($j = 3$)   ($j = 4$)

(e) trajectories of movement $T_m = 5$ (f) trajectories of movement $T_m = 6$ (g) trajectories of movement $T_m = 7$ (h) trajectories of movement $T_m = 8$
($j = 1$)   ($j = 2$)   ($j = 3$)   ($j = 4$)
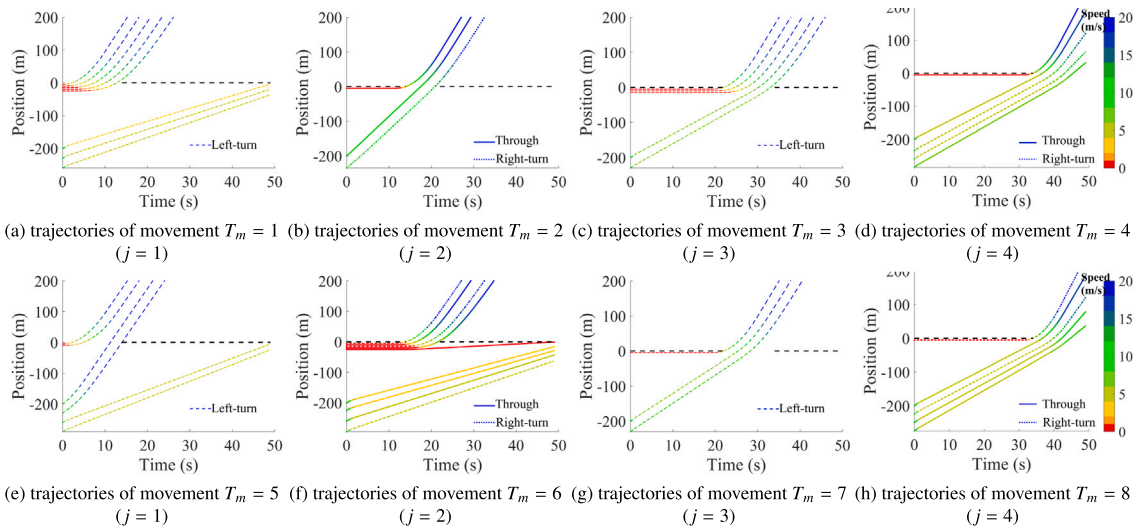
Fig. 5. Optimal performance under Scenario 3.

the cycle, i.e., the signals are longer than or equal to the aforementioned benchmark signal values. The optimal signals under the undersaturated traffic flow are demonstrated as the diamond markers in Fig. 7 and also in the bold numbers of Tables 5 and 6.

First, the optimal signal pattern in the undersaturated traffic flow with the balanced arrival rates is explored. The optimal signals tend to fix P_1 as the benchmark value, and then distribute more green time to the latter signal phases in the undersaturated traffic flow. As the bold numbers in Tables 5 and 6, P_1 is always optimized to obey the benchmark signals when $T_m^{max} = 6$ and $T_m^{max} = 8$, while P_2 and P_3 partially deviate from the benchmark values. This observation also holds for $T_m^{max} = 4$. Two signal phases ($J = 2$) with the cycle length of 40 s to 60 s are sufficient to release all vehicles, so P_1 under $T_m^{max} = 4$ is always optimized to switch as the benchmark signals, as can be seen in Fig. 7. It can be concluded that P_1 is independent of the signal cycle lengths and the signal phase numbers under the undersaturated traffic flow.

However, the optimal signal performance in the oversaturated traffic flow with the balanced vehicle arrival rates is different, as shown in the phase lengths without markers in Fig. 7 and the normal numbers in Tables 5 and 6. The joint controller tends to allocate more green time to the signal phases in middle (e.g., P_2 or P_3). On one hand, the approaching vehicles in the movement of $T_m = 1$ have to utilize the green time to catch up with the queuing vehicles. This however is not a problem for the approaching vehicles of movements $T_m = 2, 3, 4$ during P_2, P_3, and P_4, because they are able to utilize the preceding red phase (at least P_1) to

(a) trajectories of movement $T_m = 1$ (b) trajectories of movement $T_m = 2$ (c) trajectories of movement $T_m = 3$ (d) trajectories of movement $T_m = 4$
($j = 1$)   ($j = 2$)   ($j = 3$)   ($j = 4$)

(e) trajectories of movement $T_m = 5$ (f) trajectories of movement $T_m = 6$ (g) trajectories of movement $T_m = 7$ (h) trajectories of movement $T_m = 8$
($j = 1$)   ($j = 2$)   ($j = 3$)   ($j = 4$)
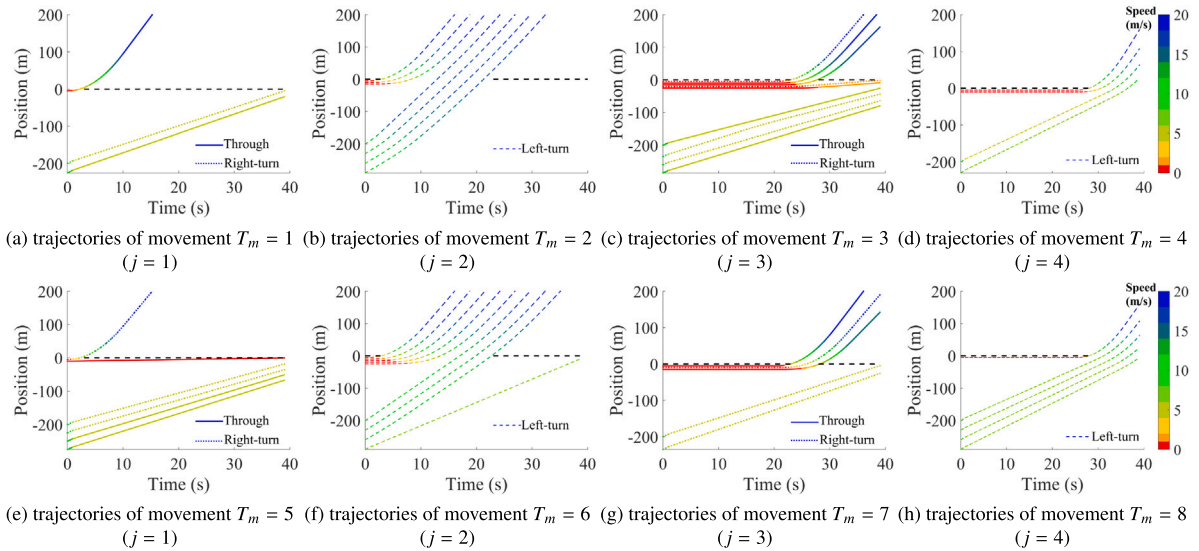
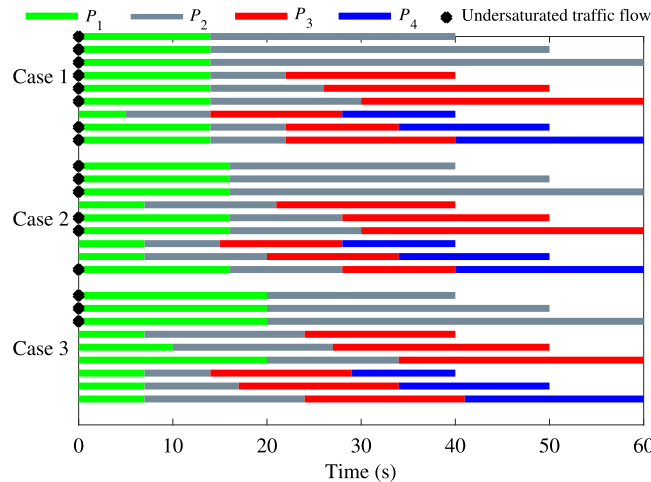**Fig. 6.** Optimal performance under Scenario 4.

Fig. 7. Optimal signals under the balanced vehicle arrival rates.

reach the stop-bar. Thus, terminating P_1 earlier results in releasing more vehicles in the later green phases in the oversaturated traffic flow. As can be seen in Scenario 2, P_1 is switched even without releasing the last queuing vehicle in Fig. 4(a), and in this way all vehicles of movements $T_m = 2, 3, 4$ are dissipated, as in Figs. 4(b) to (d). On the other hand, the arrival speeds of the approaching vehicles in the last signal phase (e.g., P_3 or P_4) are lower compared to the counterparts in other signal phases, as discussed in the vehicle trajectory pattern. In other words, the signal phases in middle (P_2 or P_3) require less green time to release one more vehicle. The last signal phase is thereby less efficient (with respect to throughput and travel delay) under the oversaturated traffic flow.

The optimal signals under the unbalanced vehicle arrival rates from different arms basically obey the abovementioned patterns, and the signals are optimized to be responsive to the unbalanced vehicle actuation, as shown in Fig. 5 of Scenario 3 and Fig. 6 of Scenario 4. The optimal signal phase lengths of P_1 to P_4 are 15 s, 6 s, 13 s and 16 s under Scenario 4, and 3 s, 12 s, 13 s and 12 s under Scenario 4. Although the optimal signals under the unbalanced vehicle arrival rates do not obviously allocate more green time to the signal phases in middle as under the balanced vehicle arrival rates, the optimal signals can react to the actuation of the controlled vehicles based on the information of speed and position. It can be concluded that the traffic signals are optimized to release the most vehicles within the cycle under the unbalanced vehicle arrival rates, thus the green time is rarely wasted without discharging any vehicle.

With an increase in the signal cycle length, the total number of passing vehicles within the cycle rises, but the objective function value decreases. Thus, the cycle length should be restricted as a constant or at least be bounded within a certain range; otherwise,

Table 5
Optimal signals under the balanced vehicle arrival rates ($T_m^{\max} = 6$).

Cycle length	Case 1 (24 veh)				Case 2 (36 veh)				Case 3 (48 veh)			
C (s)	P_1	P_2	P_3	Released vehicles	P_1	P_2	P_3	Released vehicles	P_1	P_2	P_3	Released vehicles
$C = 40$	14	8	18	24 veh	7	14	19	30 veh	7	17	16	38 veh
$C = 41$	14	8	19	24 veh	7	14	20	30 veh	7	17	17	38 veh
$C = 42$	14	8	20	24 veh	7	15	20	30 veh	7	17	18	38 veh
$C = 43$	14	8	21	24 veh	7	15	21	30 veh	7	17	19	38 veh
$C = 44$	14	9	21	24 veh	16	12	16	36 veh	7	17	20	38 veh
$C = 45$	14	9	22	24 veh	16	12	17	36 veh	7	17	21	38 veh
$C = 46$	14	10	22	24 veh	16	12	18	36 veh	7	17	22	38 veh
$C = 47$	14	10	23	24 veh	16	12	19	36 veh	7	17	23	38 veh
$C = 48$	14	11	23	24 veh	16	12	20	36 veh	7	18	23	38 veh
$C = 49$	14	11	24	24 veh	16	12	21	36 veh	7	18	24	38 veh
$C = 50$	14	12	24	24 veh	16	12	22	36 veh	10	17	23	40 veh
$C = 51$	14	12	25	24 veh	16	12	23	36 veh	10	17	24	40 veh
$C = 52$	14	13	25	24 veh	16	12	24	36 veh	10	17	25	40 veh
$C = 53$	14	13	26	24 veh	16	12	25	36 veh	10	17	26	40 veh
$C = 54$	14	14	26	24 veh	16	12	26	36 veh	15	17	22	44 veh
$C = 55$	14	14	27	24 veh	16	12	27	36 veh	20	14	21	46 veh
$C = 56$	14	15	27	24 veh	16	13	27	36 veh	20	14	22	46 veh
$C = 57$	14	15	28	24 veh	16	13	28	36 veh	20	14	23	46 veh
$C = 58$	14	16	28	24 veh	16	14	28	36 veh	20	14	24	46 veh
$C = 59$	14	16	29	24 veh	16	14	29	36 veh	20	14	25	46 veh
$C = 60$	14	16	30	24 veh	16	14	30	36 veh	20	14	26	46 veh

Table 6
Optimal signals under the balanced vehicle arrival rates ($T_m^{\max} = 8$).

Cycle length	Case 1 (32 veh)					Case 2 (48 veh)					Case 3 (64 veh)				
C (s)	P_1	P_2	P_3	P_4	Released vehicles	P_1	P_2	P_3	P_4	Released vehicles	P_1	P_2	P_3	P_4	Released vehicles
$C = 40$	5	9	14	12	28 veh	7	8	13	12	38 veh	7	7	15	11	38 veh
$C = 41$	5	9	14	13	28 veh	7	8	13	13	38 veh	7	7	17	10	40 veh
$C = 42$	5	9	14	14	28 veh	7	10	12	13	40 veh	7	7	17	11	40 veh
$C = 43$	5	10	15	13	28 veh	7	13	12	11	42 veh	5	10	17	11	40 veh
$C = 44$	5	10	15	14	28 veh	7	13	12	12	42 veh	5	10	17	12	42 veh
$C = 45$	5	10	15	15	28 veh	7	13	12	13	42 veh	5	10	17	13	42 veh
$C = 46$	14	8	10	14	32 veh	7	13	12	14	42 veh	7	12	14	13	44 veh
$C = 47$	14	8	10	15	32 veh	7	13	12	15	42 veh	7	12	14	14	46 veh
$C = 48$	14	8	10	16	32 veh	7	13	12	16	42 veh	7	12	14	15	46 veh
$C = 49$	14	8	12	15	32 veh	7	13	14	15	42 veh	7	10	17	15	46 veh
$C = 50$	14	8	12	16	32 veh	7	13	14	16	42 veh	7	10	17	16	48 veh
$C = 51$	14	8	12	17	32 veh	7	13	14	17	42 veh	7	10	17	17	48 veh
$C = 52$	14	8	14	16	32 veh	7	13	16	16	42 veh	7	17	14	14	50 veh
$C = 53$	14	8	14	17	32 veh	7	13	16	17	42 veh	7	17	14	15	50 veh
$C = 54$	14	8	14	18	32 veh	7	13	16	18	42 veh	7	17	14	16	52 veh
$C = 55$	14	8	16	17	32 veh	16	12	12	15	48 veh	7	17	14	17	52 veh
$C = 56$	14	8	16	18	32 veh	16	12	12	16	48 veh	7	17	14	18	52 veh
$C = 57$	14	8	16	19	32 veh	16	12	12	17	48 veh	7	17	14	19	52 veh
$C = 58$	14	8	18	18	32 veh	16	12	12	18	48 veh	7	17	17	17	54 veh
$C = 59$	14	8	18	19	32 veh	16	12	12	19	48 veh	7	17	17	18	54 veh
$C = 60$	14	8	18	20	32 veh	16	12	12	20	48 veh	7	17	17	19	54 veh

the signal optimization will extend the current cycle as long as possible. In addition, the signal phase lengths in Tables 5 and 6 show the tendency that the moments of switching signals are normally the same under similar signal cycle lengths.

From the discussion above, the joint controller is capable of incorporating different traffic demand levels and signal designs, determining signals for the optimal performance of all vehicles from multiple movements in the control zone. The optimal signal pattern can provide design insights into engineering implementations. For instance, the first signal phase length P_1 can be pre-determined using the empirical data in the undersaturated traffic flow with balanced vehicle arrival rates, which can relieve the computational time to some extent.

4.3. Computational performance analysis

In this subsection, the computational performance of the proposed joint controller is analyzed, considering the dimension of control variables and the average running time under different traffic demand levels, the released traffic movement numbers and signal cycle lengths. The mean computational time is calculated by averaging ten runtimes on the desktop of Intel(R) Core(TM) i7-9700 K CPU with 16 GB memory.
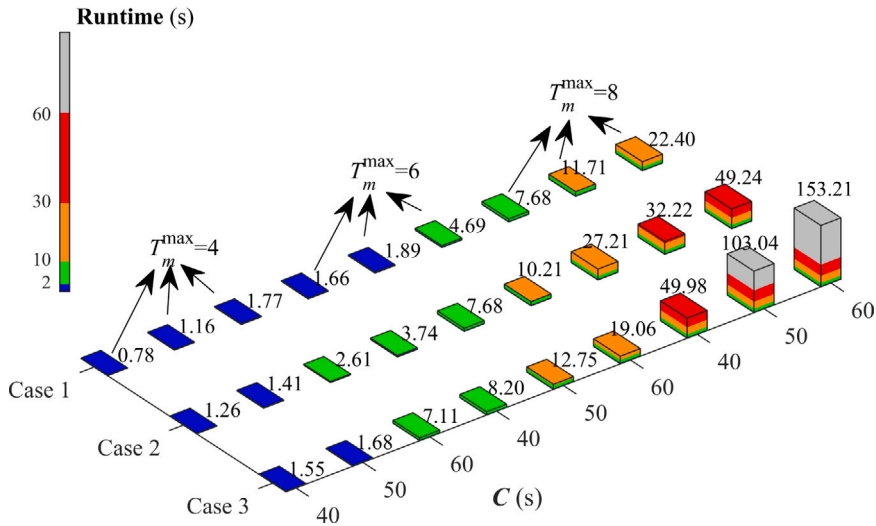
Fig. 8. Average computational time under the balanced arrival rates.
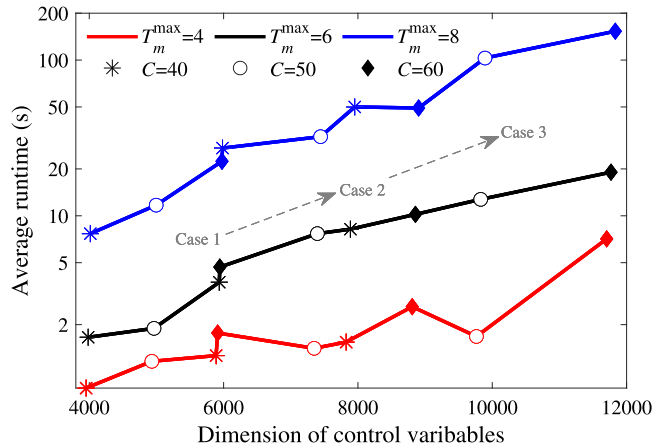

Fig. 9. The relationship between the computational time and the control variable dimension.

The average computational time under the balanced arrival rates is detailed in Fig. 8. In the horizontal plane of Fig. 8, the southwestern coordinate presents Case 1 to Case 3, and the southeastern coordinate implies the cycle lengths of 40 s, 50 s and 60 s under the maximal released traffic movement number $T_m^{\max} = 4, 6, 8$. The vertical coordinate shows the average runtime in color, as demonstrated in the colorbar. The blue, green and orange bars represent the runtime sections of 0 to 2 s, 2 s to 10 s, and 10 s to 30 s respectively, the total of which account for the majority of all runtimes. The longest mean running time, 153,21 s, occurs under Case 3 when $C = 60$ s and $T_m^{\max} = 8$. It is obvious that the increases in the released movements T_m, signal cycle lengths C and vehicle numbers N result in longer runtime. The optimal signal patterns stay unchanged in all experiments.

The relationship between the computational time and the control variable dimension is revealed in Fig. 9. The vertical axis is presented compactly by way of the exponential scale. The horizontal axis shows the dimension of control variables, which ascends with the increases in the released movement numbers (see line colors), cycle lengths (see line markers), and Case 1 to Case 3 (see the gray dashed arrows). The cycle lengths with same markers on a certain line are distinguished by the case number, as the gray arrows from the left bottom to the top right. As can be seen, the average runtime normally undergoes the exponential growth when control dimensions increase.

4.4. Comparison analysis

In order to demonstrate the advantages of the joint controller, the comparison is made between the proposed approach and five other approaches, i.e., the Intelligent Driver Model (IDM), the Webster model, the capacity factor maximization model (Cantarella and Improta, 1988), the delay minimization model (Improta and Cantarella, 1984), and the state of the art in Xu et al. (2018).
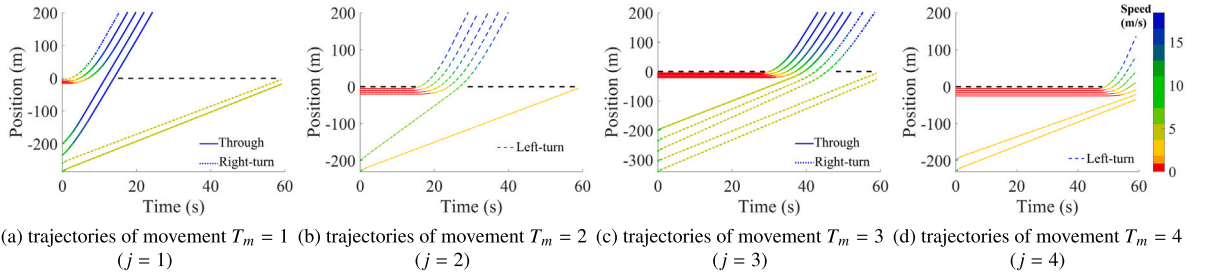
(a) trajectories of movement $T_m = 1$ (b) trajectories of movement $T_m = 2$ (c) trajectories of movement $T_m = 3$ (d) trajectories of movement $T_m = 4$
    ($j = 1$)   ($j = 2$)   ($j = 3$)   ($j = 4$)

Fig. 10. The performance of the comparison case II.

The comparison scenario is designed similarly as Scenario 4. The left-turn movement is released afterwards with various turning proportions under the unbalanced vehicle arrival rates. The controlled vehicle numbers per movement are generated in the same way as in Scenario 4. The only differences are the cycle length of $C = 60$ s and the controlled vehicle number of $N = 64$. The same parameter values and settings are applied in all comparison cases.

The comparison cases are listed in Table 7. In comparison cases I to IV, the signal parameters are calculated in the upper layer using the Webster model, the capacity factor maximization model, and the delay minimization model respectively. In the lower layer which treats the signal parameters generated from the upper layer as inputs, vehicle trajectories in the comparison case I are determined using IDM, while trajectories are optimized in comparison cases II to IV using Eqs. (1) to (5), (11), (13) to (16), (27) to (31) to diminish the differences resulted from the trajectory optimization. The comparison case V jointly optimizes vehicle trajectories and traffic signals using the state-of-the-art approach (Xu et al., 2018), which excludes the stopping vehicles in the control design so they are removed in implementation. Finally, the comparison case VI aims at verifying the benefits of the proposed joint control approach. The performance of comparison cases II, V, and VI is illustrated in Figs. 10–12. For concise presentation, the movements of $T_m = 5, 6, 7, 8$ are not shown. The comparison cases III and IV are not presented owing to the similar performance as case II, resulted from the similar signal parameter values and the same trajectory optimization model.

The indicator of travel delay is calculated by vehicle arrival time minus the minimal traveling time from the initial position to the stop-bar (e.g., traveling with the limit speed v_{max}). Throughput is the number of vehicles that can pass the intersection within the current signal cycle. The VT-Micro model of Rakha et al. (2004) is adopted to calculate the HC emission. The instantaneous fuel consumption model in Kamal et al. (2011) and the traveling distance are applied to calculate the fuel consumption in ml/m. The fuel consumption rate (ml/s) can be estimated by

$$f_{eco} = \begin{cases} b_0 + b_1 v_{ij}(k) + b_2 v_{ij}^2(k) + b_3 v_{ij}^3(k) + a_{ij}(k)\left(c_0 + c_1 v_{ij}(k) + c_2 v_{ij}^2(k)\right) & a_{ij}(k) > 0 \\ b_0 + b_1 v_{ij}(k) + b_2 v_{ij}^2(k) + b_3 v_{ij}^3(k) & a_{ij}(k) \le 0 \end{cases} \tag{32}$$

The indicator values of throughput, delay, fuel consumption, and emission are detailed in Table 7 (stopping vehicles in the state-of-the-art approach are excluded). The proposed control approach outperforms the other strategies of cases I to V in throughput and delay, and the proposed approach performs well on fuel consumption and emission, which proves the superiority of the proposed controller. The advantages of the proposed control approach over the signal-only optimization are revealed by comparing case I with case VI. The benefits of the joint optimization between trajectories and signals over the trajectory-only optimization can be demonstrated by the differences of indicator values between cases II to IV and cases V to VI. The advantages of the trajectory optimization model in this paper are explored by the comparison between case I and case II. The benefits of the proposed approach over the state-of-the-art approach, which excludes all stopping vehicles, are verified by comparing case V with case VI.

Furthermore, the signal parameters generated from different signal control methods (comparison cases I to IV) are almost the same, because these signal optimization models generally reflect the traffic flow ratios. As a result, there are only minor differences in the values of all indicators among comparison cases II to IV. On the contrary, the proposed control approach can not only consider vehicle arrival rates but also take vehicle speeds and positions into account to release more vehicles during the green phases, which have been discussed in subsections 4.2.1 and 4.2.2.

4.5. Discussion

The proposed controller jointly optimizes cooperative vehicle trajectories and traffic signal parameters at a standard four-arm signalized intersection with a predefined phase sequence, providing perfect V2V and I2V communication. It is observed from simulation results that the control objectives are fulfilled and all constraints are satisfied under different traffic demand levels with the balanced or unbalanced arrival rates from different legs, and the proposed controller has the flexibility in incorporating various cycle lengths, signal phase sequences, and turning proportions. Furthermore, the optimal trajectory and signal patterns are discovered based on the optimal performance of the joint controller. Multiple runs of different experiments show the generalizability of the proposed controller.

The dimensionality of the control problem will dramatically rise with the increase in vehicle numbers, resulting in long runtime. This is the main limitation of the proposed controller. A high performance computer is able to reduce the computational time and possibly solve this problem in real time. Decentralized computation approach can also contribute to expediting the solution time, which will be studied in the future to implement the joint control approach in real time.
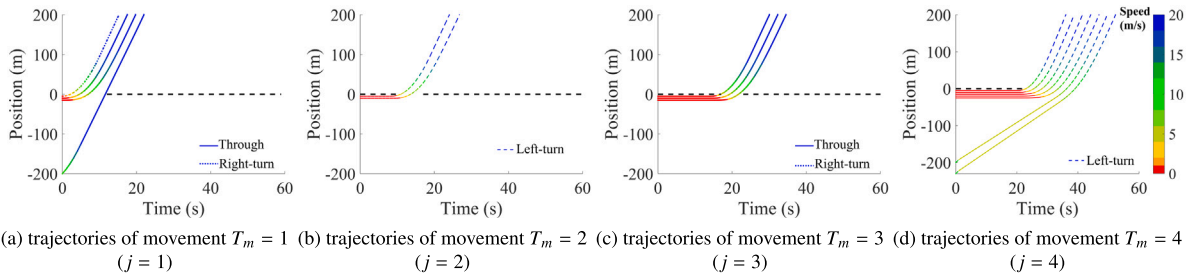
(a) trajectories of movement $T_m = 1$ (b) trajectories of movement $T_m = 2$ (c) trajectories of movement $T_m = 3$ (d) trajectories of movement $T_m = 4$
($j = 1$)   ($j = 2$)   ($j = 3$)   ($j = 4$)

Fig. 11. The performance of the comparison case V.

(a) trajectories of movement $T_m = 1$ (b) trajectories of movement $T_m = 2$ (c) trajectories of movement $T_m = 3$ (d) trajectories of movement $T_m = 4$
($j = 1$)   ($j = 2$)   ($j = 3$)   ($j = 4$)
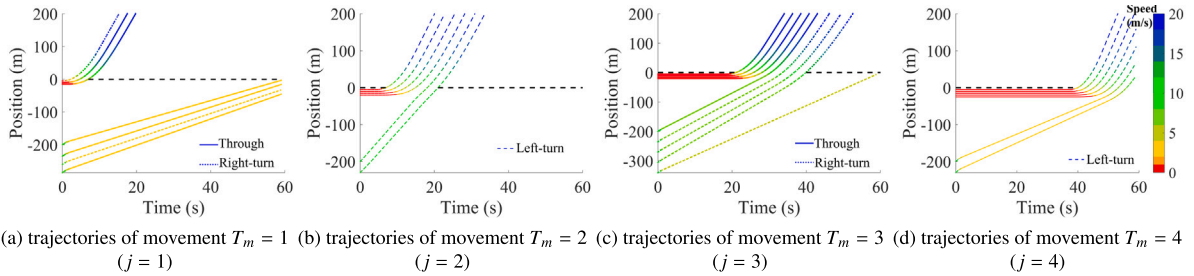
Fig. 12. The performance of the comparison case VI.

Table 7
Indicators of the comparison cases.

	Signal control	Trajectory	Phase lengths (s) (P_1 to P_4)	Throughput (veh)	Delay (s/veh)	Fuel consumption (ml/m)	Emission (HC: g/km)
Case I	Webster model	IDM	15.69, 13.94, 19.17, 11.20	32	38.76	0.0814	0.0118
Case II	Webster model	Optimization	15.69, 13.94, 19.17, 11.20	41	34.62	0.0742	0.0106
Case III	Capacity factor maximization model	Optimization	15.43, 13.71, 18.86, 12.00	45	33.05	0.0739	0.0109
Case IV	Delay minimization model	Optimization	15.07, 15.49, 13.94, 15.50	45	33.18	0.0743	0.0108
Case V	Joint optimization of state-of-the-art (only passing vehicles)		12, 6, 6, 36	31	34.87	0.0692	0.0123
Case VI	Joint optimization of the proposed approach		7, 14, 19, 20	46	31.04	0.0739	0.0108

5. Conclusions and future work

In this paper, we propose a joint control approach that simultaneously optimizes traffic signals and vehicle trajectories at isolated intersections in a cooperative vehicle environment. The objective of the proposed approach is to release as many vehicles as possible with ride comfort during the signal cycle (i.e., maximize comfort and minimize travel delay of the overall controlled platoons) by determining vehicle accelerations and signal phase lengths. The physical speeds, admissible accelerations, the safe gap requirement are imposed as linear constraints. The red phase logic constraints are recast into linear position constraints, which enables determining signal changes as vehicle-level variables without the need of the pre-specified terminal conditions on speed and position at the cycle tail. Our approach formulates the joint signal and trajectory control problem into a single-layer mixed linear integer framework, which bypasses the process of simulating vehicle trajectories when evaluating feasible signal plans and can be solved by standard solvers.

The flexibility of the joint control approach is revealed when integrating multiple traffic movements under different traffic demand levels. Simulation under various scenarios is conducted at a standard four-arm intersection to validate the performance of the joint control approach considering the balanced/unbalanced vehicle arrival rates and different signal phase sequences. The simulation results demonstrate the characteristics of the optimal signals and the platoon performance of splitting, merging, accelerating and decelerating. Typical vehicle trajectories and the optimal signal performance can be extracted from the optimal trajectory and signal patterns respectively, and then be applied in similar control problems. Furthermore, the comparison is made with the two-layer approaches using the car following model, the signal optimization models, and the state-of-the-art approach, which demonstrate the benefits of the proposed approach in throughput, travel delay, fuel consumption, and emission.

Further research is directed to reducing the computational time of the optimization model for real-time control, and handling detection errors and uncertainties. The applicability under the sophisticated phasing plans (e.g., optimization of phase sequence)

and intersection configuration designs will be verified in the next research step. Refining the design framework in the mixed traffic with human-driven vehicles and the extension to a corridor or a network level are also relevant topics for future research.

CRediT authorship contribution statement

Meiqi Liu: Conceptualization, Methodology, Mathematical formulation, Writing – original draft, Visualization, Investigation, Writing – review & editing. **Jing Zhao:** Mathematical formulation, Writing – review & editing. **Serge Hoogendoorn:** Supervision. **Meng Wang:** Conceptualization, Methodology, Mathematical formulation, Writing – review & editing.

Acknowledgments

References

Ahmane, M., Abbas-Turki, A., Perronnet, F., Wu, J., El Moudni, A., Buisson, J., Zeo, R., 2013. Modeling and controlling an isolated urban intersection based on cooperative vehicles. Transp. Res. C 28, 44–62.

Al Islam, S.B., Hajbabaie, A., 2017. Distributed coordinated signal timing optimization in connected transportation networks. Transp. Res. C 80, 272–285.

Altan, O.D., Wu, G., Barth, M.J., Boriboonsomsin, K., Stark, J.A., 2017. Glidepath: Eco-friendly automated approach and departure at signalized intersections. IEEE Trans. Intell. Vehicles 2 (4), 266–277.

Asadi, B., Vahidi, A., 2010. Predictive cruise control: Utilizing upcoming traffic signal information for improving fuel economy and reducing trip time. IEEE Trans. Control Syst. Technol. 19 (3), 707–714.

Beak, B., Head, K.L., Feng, Y., 2017. Adaptive coordination based on connected vehicle technology. Transp. Res. Rec. 2619 (1), 1–12.

Burger, M., Van Den Berg, M., Hegyi, A., De Schutter, B., Hellendoorn, J., 2013. Considerations for model-based traffic control. Transp. Res. C 35, 1–19.

Cantarella, G.E., Improta, G., 1988. Capacity factor or cycle time optimization for signalized junctions: a graph theory approach. Transp. Res. B 22 (1), 1–23.

Chen, S., Sun, D.J., 2016. An improved adaptive signal control method for isolated signalized intersection based on dynamic programming. IEEE Intell. Transp. Syst. Mag. 8 (4), 4–14.

Feng, Y., Head, K.L., Khoshmagham, S., Zamanipour, M., 2015. A real-time adaptive signal control in a connected vehicle environment. Transp. Res. C 55, 460–473.

Feng, Y., Yu, C., Liu, H.X., 2018. Spatiotemporal intersection control in a connected and automated vehicle environment. Transp. Res. C 89, 364–383.

Guo, Q., Li, L., Ban, X.J., 2019a. Urban traffic signal control with connected and automated vehicles: A survey. Transp. Res. C 101, 313–334.

Guo, Y., Ma, J., Xiong, C., Li, X., Zhou, F., Hao, W., 2019b. Joint optimization of vehicle trajectories and intersection controllers with connected automated vehicles: Combined dynamic programming and shooting heuristic approach. Transp. Res. C 98, 54–72.

Hao, P., Wu, G., Boriboonsomsin, K., Barth, M.J., 2018. Eco-approach and departure (EAD) application for actuated signals in real-world traffic. IEEE Trans. Intell. Transp. Syst. 20 (1), 30–40.

He, X., Liu, H.X., Liu, X., 2015. Optimal vehicle speed trajectory on a signalized arterial with consideration of queue. Transp. Res. C 61, 106–120.

HomChaudhuri, B., Vahidi, A., Pisu, P., 2016. Fast model predictive control-based fuel efficient control strategy for a group of connected vehicles in urban road conditions. IEEE Trans. Control Syst. Technol. 25 (2), 760–767.

Improta, G., Cantarella, G., 1984. Control system design for an individual signalized junction. Transp. Res. B 18 (2), 147–167.

Jiang, H., Hu, J., An, S., Wang, M., Park, B.B., 2017. Eco approaching at an isolated signalized intersection under partially connected and automated vehicles environment. Transp. Res. C 79, 290–307.

Kamal, M.A.S., Mukai, M., Murata, J., Kawabe, T., 2011. Ecological vehicle control on roads with up-down slopes. IEEE Trans. Intell. Transp. Syst. 12 (3), 783–794.

Kamal, M.A.S., Mukai, M., Murata, J., Kawabe, T., 2012. Model predictive control of vehicles on urban roads for improved fuel economy. IEEE Trans. Control Syst. Technol. 21 (3), 831–841.

Le, T., Kovács, P., Walton, N., Vu, H.L., Andrew, L.L., Hoogendoorn, S.S., 2015. Decentralized signal control for urban road networks. Transp. Res. C 58, 431–450.

Lee, J., Park, B., 2012. Development and evaluation of a cooperative vehicle intersection control algorithm under the connected vehicles environment. IEEE Trans. Intell. Transp. Syst. 13 (1), 81–90.

Lee, J., Yu, Z., 1994. Tuning of model predictive controllers for robust performance. Comput. Chem. Eng. 18 (1), 15–37.

Li, W., Ban, X., 2018. Connected vehicles based traffic signal timing optimization. IEEE Trans. Intell. Transp. Syst. 20 (12), 4354–4366.

Li, J., Dridi, M., El-Moudni, A., 2014a. Multi-vehicles green light optimal speed advisory based on the augmented lagrangian genetic algorithm. In: 17th International IEEE Conference on Intelligent Transportation Systems, ITSC. IEEE, pp. 2434–2439.

Li, Z., Elefteriadou, L., Ranka, S., 2014b. Signal control optimization for automated vehicles at isolated signalized intersections. Transp. Res. C 49, 1–18.

Li, X., Ghiasi, A., Xu, Z., Qu, X., 2018. A piecewise trajectory optimization model for connected automated vehicles: Exact optimization algorithm and queue propagation analysis. Transp. Res. B 118, 429–456.

Liu, M., Hoogendoorn, S., Wang, M., 2020. Receding horizon cooperative platoon trajectory planning on corridors with dynamic traffic signal. Transp. Res. Rec. 0361198120954869.

Liu, M., Wang, M., Hoogendoorn, S., 2019. Optimal platoon trajectory planning approach at arterials. Transp. Res. Rec. 2673 (9), 214–226.

Liu, M., Zhao, J., Hoogendoorn, S., Wang, M., 2021. An optimal control approach of integrating traffic signals and cooperative vehicle trajectories at intersections. Transportmetrica B (1-17).

Niroumand, R., Tajalli, M., Hajibabai, L., Hajbabaie, A., 2020. Joint optimization of vehicle-group trajectory and signal timing: Introducing the white phase for mixed-autonomy traffic stream. Transp. Res. C 116, 102659.

Rakha, H., Ahn, K., Trani, A., 2004. Development of VT-Micro model for estimating hot stabilized light duty vehicle and truck emissions. Transp. Res. D 9 (1), 49–74.

Stebbins, S., Hickman, M., Kim, J., Vu, H.L., 2017. Characterising green light optimal speed advisory trajectories for platoon-based optimisation. Transp. Res. C 82, 43–62.

Stevanovic, A., Stevanovic, J., Kergaye, C., 2013. Green light optimized speed advisory systems: Impact of signal phasing information accuracy. Transp. Res. Rec. 2390 (1), 53–59.

Typaldos, P., Papamichail, I., Papageorgiou, M., 2020. Minimization of fuel consumption for vehicle trajectories. IEEE Trans. Intell. Transp. Syst. 21 (4), 1716–1727.

Wan, N., Vahidi, A., Luckow, A., 2016. Optimal speed advisory for connected vehicles in arterial roads and the impact on mixed traffic. Transp. Res. C 69, 548–563.

Wang, M., Hoogendoorn, S.P., Daamen, W., van Arem, B., Happee, R., 2015. Game theoretic approach for predictive lane-changing and car-following control. Transp. Res. C 58, 73–92.

Wang, Z., Wu, G., Barth, M.J., 2019. Cooperative eco-driving at signalized intersections in a partially connected and automated vehicle environment. IEEE Trans. Intell. Transp. Syst. 21 (5), 2029–2038.

Xu, B., Ban, X.J., Bian, Y., Li, W., Wang, J., Li, S.E., Li, K., 2018. Cooperative method of traffic signal optimization and speed control of connected vehicles at isolated intersections. IEEE Trans. Intell. Transp. Syst. 20 (4), 1390–1403.

Yang, K., Guler, S.I., Menendez, M., 2016. Isolated intersection control for various levels of vehicle technology: Conventional, connected, and automated vehicles. Transp. Res. C 72, 109–129.

Yu, C., Feng, Y., Liu, H.X., Ma, W., Yang, X., 2018. Integrated optimization of traffic signals and vehicle trajectories at isolated urban intersections. Transp. Res. B 112, 89–112.

Yu, C., Sun, W., Liu, H.X., Yang, X., 2019. Managing connected and automated vehicles at isolated intersections: From reservation-to optimization-based methods. Transp. Res. B 122, 416–435.

Zhao, J., Knoop, V.L., Wang, M., 2020. Two-dimensional vehicular movement modelling at intersections based on optimal control. Transp. Res. B 138, 1–22.

Zhao, W., Ngoduy, D., Shepherd, S., Liu, R., Papageorgiou, M., 2018. A platoon based cooperative eco-driving model for mixed automated and human-driven vehicles at a signalised intersection. Transp. Res. C 95, 802–821.

Zohdy, I.H., Rakha, H.A., 2016. Intersection management via vehicle connectivity: The intersection cooperative adaptive cruise control system concept. J. Intell. Transp. Syst. 20 (1), 17–32.